INT. J. REMOTE SENSING, 2002, VOL. 23, NO. 19, 3991–4018

Taylor & Francis
Taylor & Francis Group

Remote sensing analysis of the land surface temperature anomaly in the sand-dune region across the Israel–Egypt border

Z. QIN†§, A. KARNIELI*† and P. BERLINER‡

†The Remote Sensing Laboratory, Dept. of Energy and Environmental Physics, J. Blaustein Institute for Desert Research, Ben Gurion University of the Negev, Sede Boker Campus, 84990, Israel
‡The Wyler Laboratory for Arid Land Conservation and Development, Dept. of Dryland Agriculture, J. Blaustein Institute for Desert Research, Ben Gurion University of the Negev, Sede Boker Campus, 84990, Israel
§The Spatial Modeling Centre, Umeå University, S-981 28 Kiruna, Sweden

(*Received 5 April 2000; in final form 25 October 2000*)

Abstract. In the sand-dune region across the Israel–Egypt border, an anomalous phenomenon of thermal variation was observed on remote sensing images: the Israeli side with much more vegetation cover has higher surface temperature than the Egyptian side, where bare sand surface prevails. The study intends to examine the phenomenon using NOAA-AVHRR and Landsat TM data. The focus is to analyse the seasonal and spatial change of land surface temperature (LST) in the border region, to verify it through ground truth measurements and to simulate the average LST change on both sides according to surface composition structure. A split window algorithm containing only two parameters (transmittance and emissivity) has been developed for retrieving LST from NOAA-AVHRR data and a mono-window algorithm is proposed for computing LST from the only one thermal band of Landsat TM data. Application of these algorithms to the available AVHRR and Landsat TM data indicates that the LST anomaly does occur not only in one day but almost all the year. In hot dry summer the Israeli side is usually about 2.5–3.5°C hotter. In wet cool winter the LST difference between the sides is not large but the Israeli side still has higher LST. The Egyptian side may have slightly higher LST when surface temperature is below 20°C, several days after heavy rain, which leads to very wet surface conditions. The sharp LST contrast disappears on night-time images. Ground truth measurements indicate that the LST contrast mainly can be attributed to the surface temperature difference on the two typical surface patterns: biogenic crust and bare sand, which have above 3°C difference in surface temperature during summer. Experiments on soil samples from the field indicate that biogenic crust and sand have emissivity values of about 0.972 and 0.954, respectively, in hot dry conditions that match the environment of the region in summer. Surface composition determination based on three methods indicates that more than 72% of the ground on the Israeli side is covered with biogenic crust and more than 80% on the Egyptian

*Author for correspondence; e-mail: karnieli@bgumail.bgu.ac.il

Paper presented at an International Workshop on 'Land Cover/Land Use Change and Water Management in Arid Regions: Remote Sensing Applications in the East'. The workshop took place at the Jacob Blaustein Institute for Desert Research, Sede Boker Campus, Ben Gurion University of the Negev between 23–27 October, 2000.

International Journal of Remote Sensing
ISSN 0143-1161 print/ISSN 1366-5901 online © 2002 Taylor & Francis Ltd
http://www.tandf.co.uk/journals
DOI: 10.1080/01431160110116310

side is bare sand. Actually, the LST anomaly can be understood as the direct result of surface composition difference, especially in biogenic crust and sand cover rate. Simulation with this surface composition difference shows that the Israeli side has steadily higher LST when the temperature of the biogenic crust is more than 1°C higher that of the sand surface, which usually occurs at moderate to high temperature levels (>30°C). When temperature is between 15 and 25°C, such as at about midnight, the two sides will have no obvious LST difference. This result is in agreement with the remote sensing observation. Therefore, it can be concluded that the vegetation cover does not contribute much to the LST contrast in comparison to the effect of the biogenic crust and sand cover.

1. Introduction

The northern part of the Israel–Egypt political border is crossed by linear sand-dunes of the same lithological unit. The sand-dunes were formed by the deposition of sand and dust transported from north African desert by strong wind. In remote sensing images of visible channels, such as in figure 1, this region is characterized by a sharp contrast between bright reflectance from the Egyptian side (Sinai) and the dark Israeli side (Negev) (Tsoar and Karnieli 1996). This contrast has been interpreted as being caused by different land surface cover structures under different land

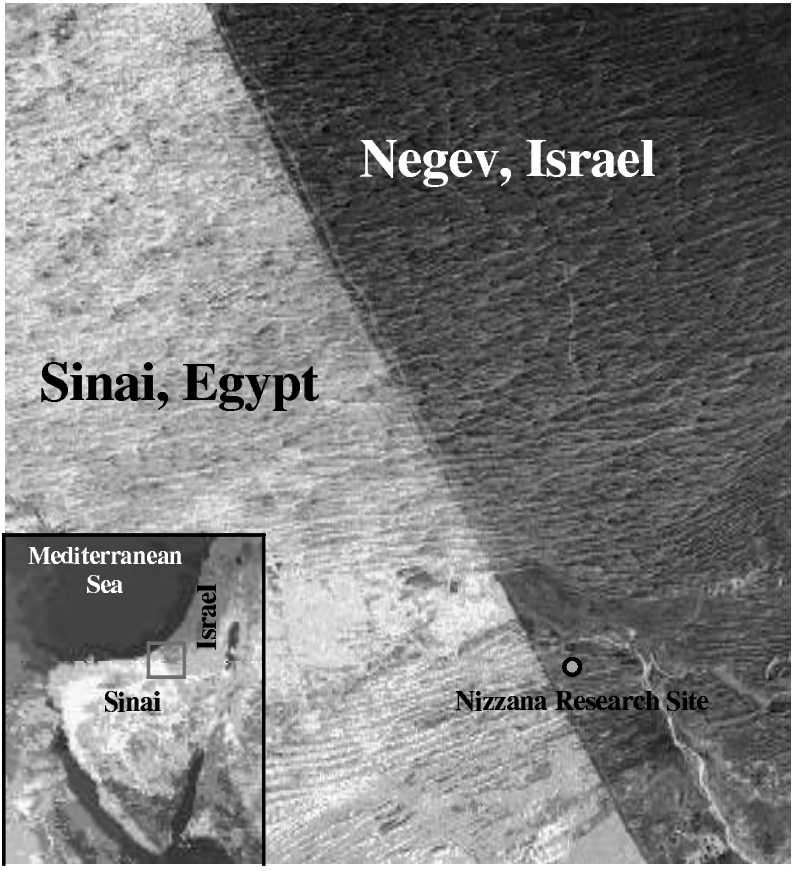

Figure 1. Landsat TM image of the sand-dune region across the Israel–Egypt border. The insert is a NOAA-AVHRR image.

use policies (Otterman 1974, 1977, 1981, Tsoar and Møller 1986). The Egyptian side has lower vegetation cover and more sand surface. On the contrast, the Israeli side is dominated by more shrubs and inactive sand surface fixed by biogenic crust, dubbed microbial crust (Kidron and Yair 1997). The thin biogenic crust (<5 mm) mainly concentrates on the lower part of the longitudinal dunes in the western Negev, and is scarce on the Egyptian side due to intensive anthropogenic activities (Tsoar and Møller 1986, Danin *et al.* 1989). Studies indicate that the biogenic crust has significant contribution to the darker reflectance on the Israeli side (Karnieli *et al.* 1996, Karnieli and Sarafis 1996). Similar spectral contrast was also observed along the border between USA and Mexico (Bahre and Bradbury 1978, Balling 1989, Balling *et al.* 1998). The United States side was darker because of its greater vegetation cover. The Mexican side is brighter because of its more sparse vegetation cover resulting from severe overgrazing activities (Balling *et al.* 1998).

In normal conditions, it might be expected that as the Israeli side contains more plants that contribute to regional evapotranspiration, it should be cooler than the Egyptian side. Such a phenomenon has been observed across the border between USA and Mexico (Balling 1989). However, the opposite was observed on the daytime thermal images of the Israel–Egypt border region, with the higher land surface temperature on the Israeli side (figure 2(a)). This phenomenon occurs not on a specific day but throughout the year, except for days when the ground is very wet and cool. Considering the higher vegetation cover on the Israeli side, this phenomenon of temperature difference in the border region is anomalous. The sharp contrast of land surface temperature (LST) cannot be seen on night-time thermal images (figure 2(b)).

The current study intends to examine the anomalous LST contrast from the viewpoint of remote sensing and ground truth measurements. Though Otterman and Tucker (1985) first mentioned this strange thermal phenomenon in their study of surface albedo in arid regions, the seasonal change and spatial variation of LST on both sides has not been analysed. This analysis was made possible by regular observation of AVHRR data from summer 1995, together with the measurement of water vapour in an atmospheric profile by CIMEL on the roof of the Remote Sensing Laboratory at Sede Boker in the southern Israeli desert. The report of Otterman and Tucker (1985) on the phenomenon was based on the direct difference of spectral scales, but not the true LST on the image they used. Actually, LST retrieval from remote sensing data requires the development of appropriate algorithms. Two algorithms for LST retrieval from AVHRR and TM data, respectively, have been developed in this study. The details have also been used for the determination of the required parameters (ground emissivity and atmospheric transmittance) for the study region. Otterman and Tucker (1985) related this thermal contrast to severe overgrazing and other anthropogenic pressures on the Egyptian side. In order to understand the LST anomaly, we conducted a number of ground truth measurements for comparison of surface temperature difference with typical surface patterns of the region, which has not been reported in the literature. Surface composition structure, which also has not been reported in literature, has been measured in this study for comparison. Based on radiance emission principle, the average LST change on both sides, which is comparable to remote sensing observation, has been simulated from the viewpoint of surface composition difference. Therefore, the study provides a thorough examination of the anomalous LST phenomenon, in order to explain its occurrence in the region.

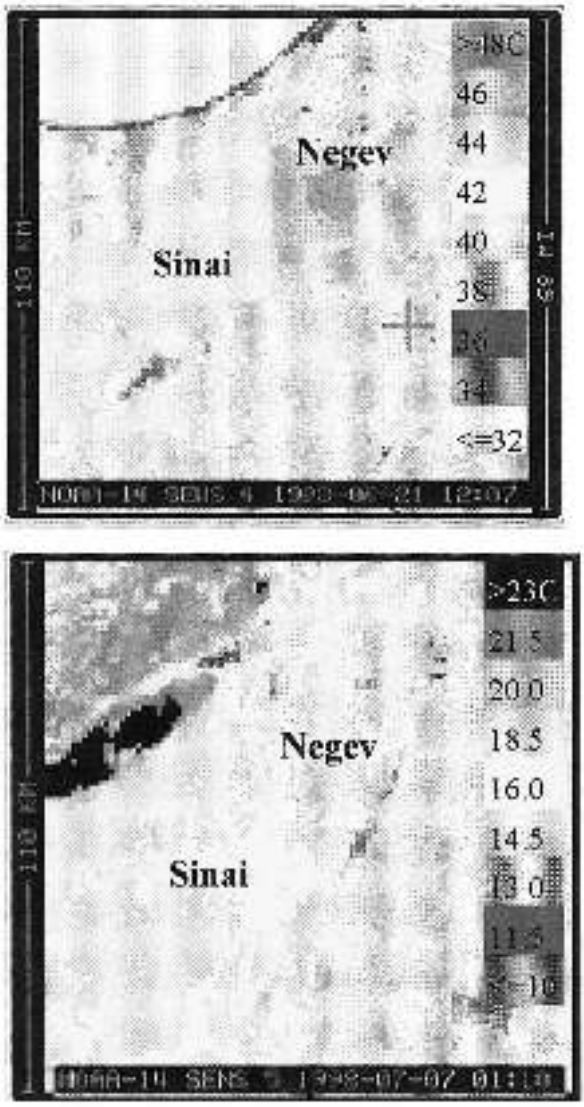

Figure 2. Daytime (a) and night-time (b) thermal images of the sand-dune region. The red cross in (a) locates Sede Boker Receiving Station in southern Israel.

2. Retrieval of LST from remote sensing data

Due to their availability, NOAA-AVHRR and Landsat Thematic Mapper (TM) data will be used in this study for analysing the temporal and spatial dynamics of the anomalous LST phenomenon in the border region. In this section, we will address the methodological aspects of retrieving LST from these two kinds of remote sensing data.

2.1. *Split window algorithm for LST retrieval from AVHRR data*

The retrieval of LST from NOAA-AVHRR data is mainly achieved through the application of split window algorithm (Vogt 1996, Qin and Karnieli 1999). The basic idea of the technique can be traced back to the early studies of sea surface temperature

from remote sensing (Prabhakara *et al.* 1974, McMillion 1975, Deschamps and Phulpin 1980). Several kinds of split window algorithm have been developed on the basis of various considerations on the atmosphere and the emitting surface (Cooper and Asrar 1989, Sobrino and Caselles 1991, Kerr *et al.* 1992). The algorithms were derived from a thermal radiance transfer equation describing the impacts of ground (mainly emissivity), atmosphere (absorption and emittance) and viewing angle on the observed thermal radiance at satellite level. The algorithms of Sobrino *et al.* (1991), França and Cracknell (1994) and Prata (1993) generally have higher accuracy but they involve some parameters that are not easy to estimate when applying to the real world (Qin *et al.* 2001a).

In the current paper, we intend to use the algorithm presented in Qin *et al.* (2001a) because it only requires two essential parameters (emissivity and transmittance) while keeping the same accuracy as the above three. After applying Taylor's expansion to linearize Planck's radiance equation with respect to temperature, Qin *et al.* (2001a) developed a new split window, having the following general form:

$$T_s = T_4 + A(T_4 - T_5) + B \tag{1}$$

where the coefficients A and B are defined as:

$$A = D_4/(D_5C_4 - D_4C_5) \tag{2}$$

$$B = [L_4D_5(1 - C_4 - D_4) - L_5D_4(1 - C_5 - D_5)\}/(D_5C_4 - D_4C_5) \tag{3}$$

$$C_i = \varepsilon_i\tau_i(\theta) \tag{4}$$

$$D_i = (1 - \tau_i(\theta))\{1 + (1 - \varepsilon_i)\tau_i(\theta)\} \tag{5}$$

Because coefficient B includes the parameter L_i, which is the function of temperature, a further derivation results in the following new form of split window algorithm:

$$T_s = A_0 + A_1T_4 - A_2T_5 \tag{6}$$

where the coefficients A_0, A_1 and A_2 are defined as:

$$A_0 = \{a_4D_5(1 - C_4 - D_4) - a_5D_4(1 - C_5 - D_5)\}/(D_5C_4 - D_4C_5) \tag{7}$$

$$A_1 = 1 + \{D_4 + b_4D_5(1 - C_4 - D_5)\}/(D_5C_4 - D_4C_5) \tag{8}$$

$$A_2 = \{D_4 + b_5D_4(1 - C_5 - D_5)\}/(D_5C_4 - D_4C_5) \tag{9}$$

The constants are given as $a_4 = -62.23928$, $a_5 = -66.54067$, $b_4 = 0.43059$ and $b_5 = 0.46585$ (Qin *et al.* 2001a). This algorithm relates the determination of the three important coefficients A_0, A_1 and A_2 to both ground emissivity and atmospheric transmittance, which are determined in §3.

Sensitivity analysis indicates that the algorithm is able to provide an accurate estimation of LST from AVHRR data. The possible LST error is only about 0.4°C due to a transmittance error of up to 0.05, and 0.71°C due to an emissivity error of 0.01, in both channels 4 and 5. Usually the estimation of transmittance and emissivity estimation can meet this accuracy requirement. Validation with both simulation data from LOWTRAN 7 and grouth truth data from Prata (1994) confirms the applicability of the algorithm (Qin *et al.* 2001a). Comparison with 11 other algorithms in the literature shows the algorithm is generally better in terms of accuracy and computation simplicity.

2.2. *Mono-window algorithm for LST retrieval from Landsat TM data*

The Landsat TM has a thermal band (band 6) with a nominal ground resolution of 120 m. This spatial resolution is much higher than the nadir ground resolution (1.1 km) of AVHHR. Therefore, it is highly suitable for use in analysing the detailed spatial patterns of LST distribution, and its difference on the two sides of the region.

Conventionally, retrieval of LST from Landsat TM6 is carried out mainly by atmospheric correction. The principle is to subtract the upward atmospheric thermal radiance and the reflected atmospheric radiance from the observed radiance at satellite level so that the brightness temperature at ground level can be directly computed. The atmospheric thermal radiance can be simulated using the LOWTRAN or MODTRAN program when the atmospheric profile is available from an *in situ* satellite pass. For many applications this is often not the case. Thus, an alternative is to use the available radiosonde data close to the satellite pass or with similar atmospheric conditions for this atmospheric simulation (Hurtado *et al.* 1996). In many cases, even the radiosonde data is not available due to difficulty of measuring. This lack of atmospheric profile *in situ* satellite pass prevents the popular application of LST retrieval from Landsat TM6 for many studies. A mono-window algorithm has been developed in Qin *et al.* (2001b) for LST retrieval from Landsat TM data. The algorithm has the following form:

$$T_s = \{a_6(1-C_6-D_6)+(b_6(1-C_6-D_6)+C_6+D_6)T_6-D_6T_a\}/C_6 \tag{10}$$

where T_a is the effective atmospheric mean temperature, which can be determined from local ground meteorological observation data by the method in Qin *et al.* (2001b), a_6 and b_6 are the constants needed to linearize Planck's radiance equation, given as $a_6 = -67.35535$ and $b_6 = 0.45861$; and the parameters C_6 and D_6 are defined as:

$$C_6 = \varepsilon_6\tau_6(\theta) \tag{11}$$

$$D_6 = (1-\tau_6(\theta))\{1+(1-\varepsilon_6)\tau_6(\theta)\} \tag{12}$$

Sensitivity analysis indicates that the error of ground emissivity has little effect on the possible LST estimation error, which is affected by atmospheric transmittance (Qin *et al.* 2001b). For an emissivity error of 0.02, the LST error is only about 0.25°C. However, for a transmittance error of 0.05, the LST error may reach to more than 1.5°C when transmittance is lower than 0.7. Therefore, a very clear sky with low water vapour content in the profile is the ideal climate for remote sensing of LST with Landsat TM. When water vapour content in the profile is less than $2\,g\,cm^{-2}$ so that the transmittance is above 0.8, the LST estimation error with this mono-window algorithm is less than 1.8°C for the combination of effects from moderate error in estimation of ground emissivity, transmittance, and atmospheric temperature. Validation to the simulation data from LOWTRAN 7 confirms the applicability of the algorithm (Qin *et al.* 2001b).

3. Determining the parameters for LST retrieval

Ground emissivity and atmospheric transmittance are extremely important parameters for the use of the above algorithms for LST retrieval from AVHRR and TM data. Therefore, they need to be carefully determined in the study. Determination of ground emissivity is mainly carried out by experiments on selected soil samples from the typical surface patterns of the field; and estimation of atmospheric transmittance mainly by atmospheric simulation with the LOWTRAN program.

3.1. *Experiments for determining ground emissivity*

Emissivity is an important factor that affects the observed surface temperature change by detecting the thermal radiation of the object under study. Though several methods have been proposed (Humes *et al.* 1994, Labed and Stoll 1991), direct measurement of emissivity of the ground surface in the field is extremely difficult due to the many factors affecting the process (Caselles *et al.* 1997). Another difficulty comes from the lack of suitable instruments. Here the assemble used by Humes *et al.* (1994) was used for the measurement. Because our study region is mainly composed of biogenic crust and bare sand, the objective of the experiment is to determine the emissivity of these two typical surface patterns.

The principle of determining emissivity through laboratory experiments is to compare the difference of radiant temperature between the measured samples and their reference black body. The experiments were done through the use of a water bath with constant temperature and a IR thermometer operating at 8–14 μm to measure the temperature of the samples. A circulator was installed in the water bath to keep temperature constant. On the top of the bath was a moveable semitransparent cover with a small hole mounting the IR thermometer so that the thermometer can be moved to point at the samples for the measurement.

The soil samples for the experiments were taken from the field of the region with metal cans. It is emphasised that the samples were taken with all care, to avoid destruction of soil structure or artificially altering its properties. The soil samples were floated on the water of the bath. Five sand samples and five biogenic crust samples were selected for the experiments. At the same time, a reference with black surface was also put in the bath. Three treatments (25°C, 35°C, and 45°C) were used for the experiments to represent the three conditions of surface temperature in the region. Since the bath was covered and the sensor is very close to the target, the effect of atmosphere is negligible. Thus, the emissivity can be estimated on the basis of Stefan-Boltzmann law as follows:

$$\varepsilon = \sigma T_o^4 / \sigma T_b^4 = (T_o / T_b)^4 \tag{13}$$

where T_b and T_o are the radiant temperatures of the black body reference and the measured object at 8–14 μm. Accordingly, ε is an average emissivity for the spectral range of 8–14 μm.

The results are shown in figure 3, and indicate that the biogenic crust has higher emissivity than sand. The average emissivity of the five samples at 25°C is 0.9671 for the biogenic crust and 0.9435 for sand. The difference is about 0.0236. The T-test was used as a successful statistical tool to test if two groups of samples are significantly different to the mean. Application of the test to the treatment yields $T_{stat} = 7.74 > T_{\alpha = 0.01} = 3.36$, indicating that the difference is statistically significant with a credibility of 99%. In the 35°C treatment, the average emissivity is 0.9702 for biogenic crust and 0.9473 for sand, with a difference of 0.0229, which is statistically significant ($T_{stat} = 10.43$). In the 45°C treatment, the emissivity of biogenic crust and sand is 0.9725 and 0.9543 respectively, with a difference of 0.0182, which is also statistically significant ($T_{stat} = 5.38$). For the region under study, the surface temperature is usually between 35–50°C at noon. Therefore, we can conclude that the surface emissivity of the biogenic crust in the region is about 0.97 and that of sand is about 0.95, with a difference of about 0.02.

The emissivity of the surface patterns can be used to estimate the average emissivity on both sides. Considering the effect of surface patterns according to their

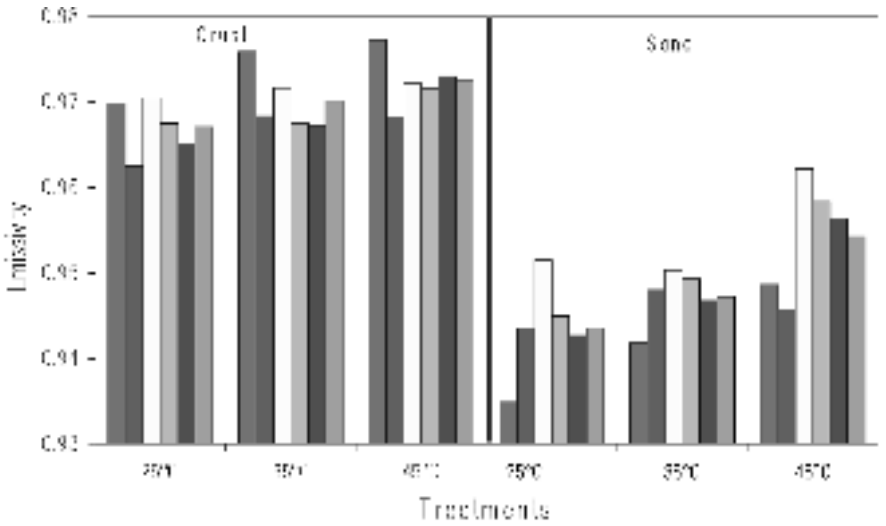

Figure 3. Emissivity of biogenic crust and sand samples for three treatments.

cover rate (see §7), the average ground emissivity of the region can be estimated as 0.968 for the Israeli side and 0.954 for the Egyptian side. Actually, emissivity also varies with wavelength and the difference of ground emissivity in the two thermal channels of AVHRR has significant impact on the accuracy of LST retrieval (Coll *et al.* 1994a). For this study, we follow the method proposed by Sobrino and Caselles (1991) to estimate ε_4 and ε_5 from ε at 8–14 μm, which gives the results as $\varepsilon_4 = 0.965$ and $\varepsilon_5 = 0.969$ for the Israel side and $\varepsilon_4 = 0.951$ and $\varepsilon_5 = 0.955$ for the Egyptian side. These results can then be used for LST retrieval from the available AVHRR data of the region. Because Landsat TM6 operates in the wavelength covering both channels 4 and 5 of AVHRR, the average emissivity of the two AVHRR channels can be served as the ground emissivity for LST retrieval from TM6 data. Thus, we have $\varepsilon_6 = 0.967$ for the Israeli side and $\varepsilon_6 = 0.953$ for the Egyptian side. The spectral contrast in visible channels allows us inserting different ground emissivity on both sides of the region for LST retrieval.

3.2. *Determination of atmospheric transmittance*

Atmospheric transmittance is a critical parameter that affects the accuracy of LST retrieval when using split-window or mono-window algorithms. The thermal radiance is attenuated on its way to the remote sensor. Transmittance depicts the magnitude of the attenuation of thermal radiance transferring through the atmosphere. The variation of atmospheric transmittance strongly depends on the dynamics of water vapour content in the profile (Sobrino *et al.* 1991, França and Cracknell 1994, Coll *et al.* 1994b). Generally, the practical way for determination of atmospheric transmittance is through simulation of local atmospheric conditions, especially water vapour content. Simulation of the relationship between atmospheric transmittance and water vapour content can be done by using atmospheric modelling programs such as LOWTRAN and MODTRAN. Here we use the LOWTRAN-7 to determine this relationship. Two atmospheric profiles are used for this simulation: high and low temperatures. The air temperature near the surface is assumed to be equal to

30°C and 18°C for high temperature, or the summer profile, and for low temperature, or the winter profile, respectively. This represents the air temperature changes in the study region. The viewing angle is also important in the simulation and for this reason an angle of 10° from the nadir was selected for AVHRR because this represents the average zenith angle of the images selected for the analysis. For Landsat TM, the image swath is about 185 km, with a zenith viewing angle of $<6°$ at the edge. Because the study region is always at the edge of available TM images, an average of 5° from nadir was used for the simulation.

Due to the arid environment, water vapour content in the atmospheric column in the study region is small. Generally speaking, it is in the range of 1.0–2.2 g cm^{-2}. In order to reveal the change of atmospheric transmittance with water vapour content, we continue the simulation for the range of 0.4–6 g cm^{-2}. Figure 4 shows the change of atmospheric transmittance with water vapour content for the two remote sensors in the high temperature profile. In the lower range of water vapour content, the relationship between water vapour content and atmospheric transmittance can be viewed as linear even though the whole is a curve as described by França and Cracknell (1994) and Sobrino *et al.* (1991). In order to generate a more accurate estimation of transmittance, we divide the whole curve into several parts and correlate them. Considering relevancy to the study area, the results are given only for 0.4–3 g cm^{-2} in table 1.

The equations listed in table 1 have very high squared correlation and low standard error, which means that the atmospheric transmittance has a strongly linear relation with water content. Standard error illustrates that the estimation of transmittance is with an accuracy of high up to $\leqslant 0.003$ by these equations. This accuracy is much higher than that estimated by a parabolic equation as proposed by França and Cracknell (1994) and Sobrino *et al.* (1991). The regression coefficients in table 1 indicate that transmittance change is within a range of 0.006–0.0164 for a small change (0.1 g cm^{-2}) of water vapour content. This means that the maximum possible

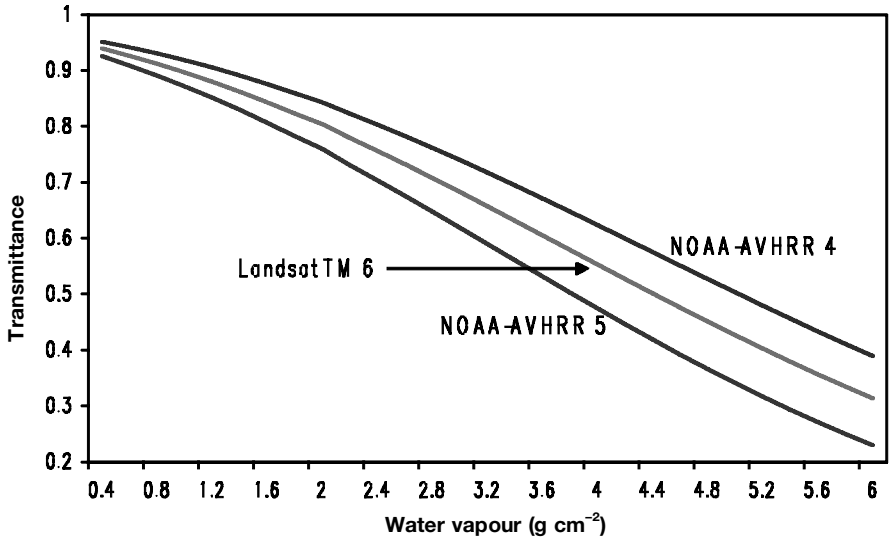

Figure 4. Total transmittance as a function of water vapour content in high temperature profile.

Table 1. Estimation of atmospheric transmittance for NOAA-AVHRR and Landsat TM.

Profiles	Water vapour (w) (g cm^{-2})	Transmittance estimation equation	Squared correlation R^2	Standard error
High temperature	0.4–1.6	$\tau_4(10) = 0.979160 - 0.062918w$	0.99425	0.002266
		$\tau_5(10) = 0.968144 - 0.098942w$	0.99716	0.002501
		$\tau_6 = 0.974290 - 0.08007w$	0.99611	0.002368
	1.6–3.0	$\tau_4(10) = 1.035378 - 0.097514w$	0.99746	0.002602
		$\tau_5(10) = 1.026468 - 0.135133w$	0.99879	0.002486
		$\tau_6 = 1.031412 - 0.11536w$	0.99827	0.002539
Low temperature	0.4–1.6	$\tau_4(10) = 0.983311 - 0.072444w$	0.99469	0.002215
		$\tau_5(10) = 0.981868 - 0.121979w$	0.99679	0.002896
		$\tau_6 = 0.982007 - 0.09611w$	0.99463	0.003340
	1.6–3.0	$\tau_4(10) = 1.058059 - 0.121354w$	0.99817	0.002749
		$\tau_5(10) = 1.048364 - 0.163678$w	0.99948	0.001973
		$\tau_6 = 1.053710 - 0.14142w$	0.99899	0.002375

error of estimation for transmittance is less than 0.033 for a probable water vapour content error of $0.2\,g\,cm^{-2}$. Usually the *in situ* measurement of atmospheric water vapour content such as CIMEL on the roof of our laboratory can meet this accuracy ($\leqslant 0.2\,g\,cm^{-2}$). For the possible water vapour content error $0.2\,g\,cm^{-2}$, the maximal estimation error of atmospheric transmittance for Landsat TM6 is <0.029.

The viewing angle is also important in determining the atmospheric transmittance of AVHRR because of its wide scanning swath (Wan and Dozier 1996). Due to the heterogeneous atmospheric conditions in each layer, the relationship between atmospheric transmittance and zenith angle is not linear but parabolic. Figure 5 clearly shows that transmittance difference from that at $\theta = 10^\circ$ increases rapidly with zenith viewing angle. Using a parabolic function to fit the curves, we get the following correction equations for AVHRR channels 4 and 5:

$$\Delta\tau_4(\theta) = (-2.399387\mathrm{E}-3) + (2.29757\mathrm{E}-5)\theta^2 \quad R^2 = 0.998487 \tag{14}$$

$$\Delta\tau_5(\theta) = (-3.276602\mathrm{E}-3) + (3.14538\mathrm{E}-5)\theta^2 \quad R^2 = 0.998729 \tag{15}$$

where $\Delta\tau_4(\theta)$ and $\Delta\tau_5(\theta)$ are atmospheric transmittance difference, and θ is the viewing anglein degrees. Therefore, for an image with θ, the transmittance is estimated as follows:

$$\tau_4(\theta) = \tau_4(10) - \Delta\tau_4(\theta) \tag{16}$$

$$\tau_5(\theta) = \tau_5(10) - \Delta\tau_5(\theta) \tag{17}$$

where $\tau_4(10)$ and $\tau_5(10)$ are the atmospheric transmittance of AVHRR channels 4 and 5 at viewing angle 10°, estimated using the equations in table 1.

4. Analysis of seasonal LST change on both sides using AVHRR data

Using the above split window algorithm and the methodology for determining its coefficients, we processed the available AVHRR data of the region for analysis of

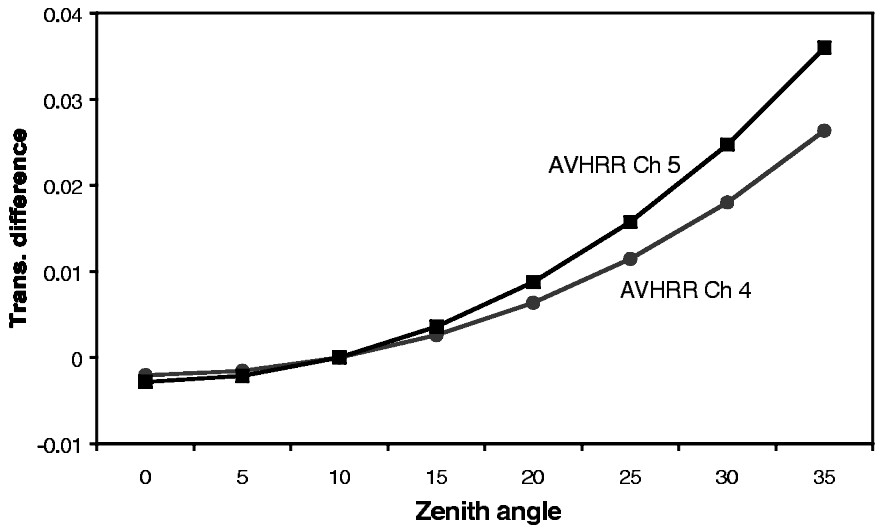

Figure 5. Atmospheric transmittance difference $\tau_i(10) - \tau_i(\theta)$as a function of zenith viewing angle.

LST change on the two sides. The images with clear sky and good viewing angle ($>60^\circ$) in the study region were selected for the processing. Since the Sede Boker Receiving Station in south Israeli desert started to acquire NOAA-AVHRR data from summer of 1995, we processed all available images to June 1999 for the analysis. All the selected daytime images for the analysis were acquired at approximately 13:00–15:30 local time. Hence the LST retrieved from these daytime images represents the temperature peak of the acquisition date. We also processed the night-time images of 1998 for analysis of the night-time LST change. All selected night-time images were acquired between 0:00 and 2:00 local time. Thus, LST retrieved from these night-time images represents the lowest temperature, at about midnight.

A rectangular subset was taken from the processed images on each side of the region for comparison. The subsets are close enough to the border to allow the assumption of similar meteorological events on both sides. The size of the subsets is 11×14 pixels, covering an area of approximately $12\,\text{km} \times 15\,\text{km}$. Subsets smaller than the whole region were used so as to be relatively homogeneous; minimizing the possible heterogeneous surface features on the two sides. The position of the subsets is shown in figure 6(a), which is an LST image of the region retrieved from NOAA-14 AVHRR data acquired at 12:08 GMT or 15:08 local time on 18 July 1998 with a viewing angle of 83.7°. The subsets were placed on the area that most represented the general surface features of each side. The average LST of the subsets was then used as the representation of the LST change on the two sides in the following analysis of the study.

4.1. *Daytime LST change and its difference on both sides*

The average LST change of the border region in 1998 is plotted in figure 7(a), and shows the seasonal change of daily maximal temperature. The climate of the region can be divided into two seasons. The hot dry season is usually May to October and the cool wet season from November to April. LST change data retrieved from daytime AVHRR images of 1998 clearly illustrate the difference between cool wet and hot dry seasons in the region. LST in the cool wet season is obviously lower. In January, daytime LST is only approximately 24°C and in December it is around 30°C. LST increases to 36–42°C in April; and it is up to 48–56°C in the hot

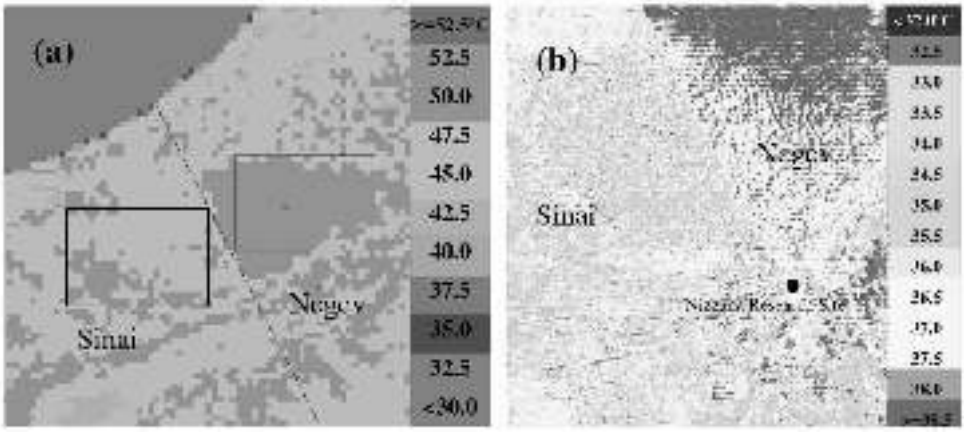

Figure 6. Spatial LST variation of the region, retrieved from (a) NOAA-AVHRR data acquired on 18 July 1998 and (b) Landsat TM data acquired on 21 September 1995.

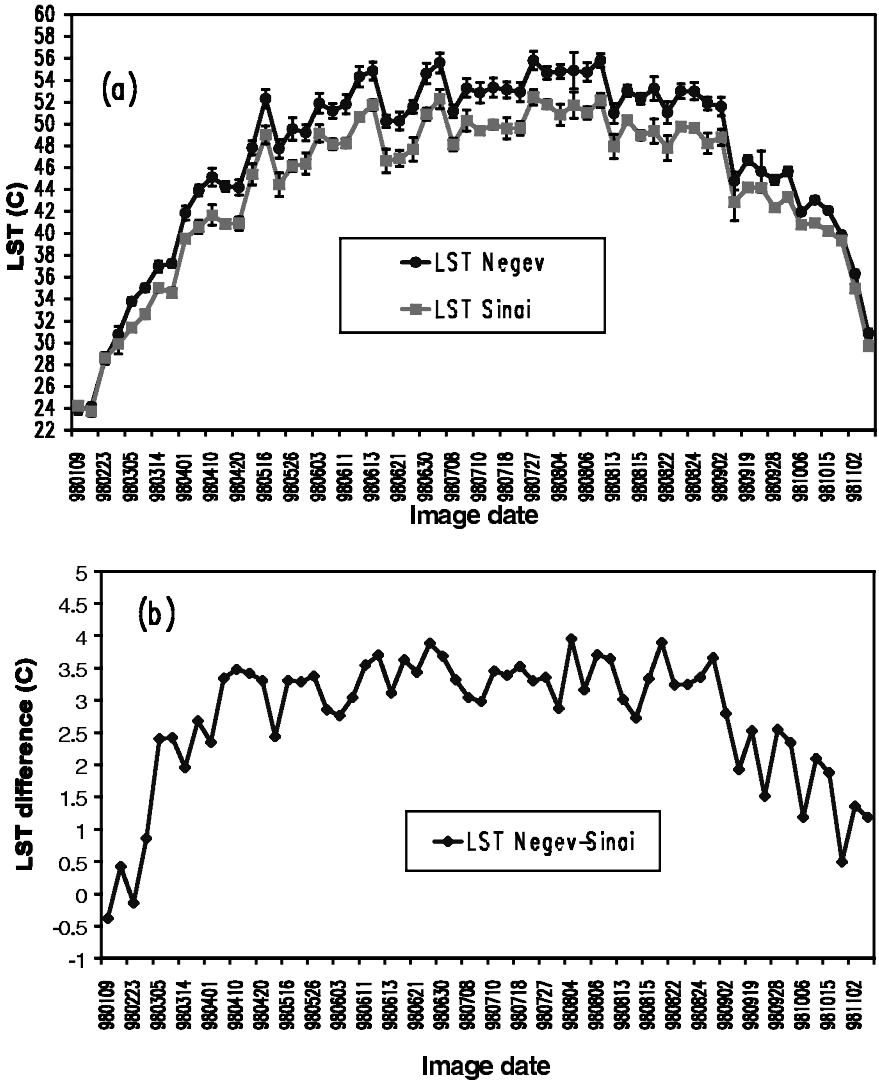

Figure 7. LST change on both sides of the region, retrieving from selected NOAA-AVHRR images of 1998. (a) Average LST change and (b) average LST difference.

dry season. Some pixels have an even higher LST than the average. The maximal LST may reach 56–60°C in summer.

After heavy rain, the ground surface for several days experiences extremely low LST (<30°C). Such examples can be seen in January 1998. There was rain on 5 January with total precipitation of 6.6 mm. Another two heavy rains with total precipitation of 23.9 mm occurred on 11 and 12 January. Therefore, it can be referred that the ground was very wet when AVHRR observed the region on 9 and 17 January. The wet surface prevented the increase of LST. Consequently, LST on these two image dates were very low (figure 7(a)). Similarly, the heavy rains on 12 (13.9 mm) and 15 February (11.2 mm) also had strong impact on the LST change observed on 23 February (figure 7(a)).

Another important feature shown in figure 7(a) is that LST on the Israeli side is always higher. A clearer illustration of LST difference across the border is given in figure 7(b), which indicates that the Israeli side is generally about 2.5–3.5°C hotter in summer. In some cases, the LST difference reaches 4°C. LST on the Israeli side is also higher in winter though the difference is not as obvious as in summer. Usually the Israeli side is about 0.5–1.5°C hotter in the cool wet season. Only in a few extreme cases when the surface was very wet after heavy rain did the Egyptian side have slightly higher LST. The LST difference in these extreme cases is generally within -0.5°C.

The LST change of the region is under the control of the seasonal climatological circle as well as the rainfall. Generally speaking, LST is high in summer and low in winter, as is clearly illustrated in figure 8, which plots the monthly average LST change from June 1995 to June 1999 and compares the change with rainfall in this period. Monthly average LST in summer is identical in 1996, 1997 and 1998, ranging from 50°C to 55°C. A slight difference can be seen in the four valleys representing the LST change in the winters. Monthly LST in winters 1996–1997 and 1997–1998 ranged from 24°C to 26°C, which was lower than in 1995–1996 and 1998–1999, when the LST was about 28–30°C. This difference can be related to the amount of rainfall and its distribution in the seasons. Rains in the cool seasons of 1995–1996 and 1998–1999 were much fewer and rain period was shorter. Consequently, average LST in these two seasons was slightly higher (figure 8).

Since most images indicate that the Israeli side has higher average LST than the Egyptian side, we also need to test if this is statistically true. The T-test yields that T_{stat} is 6.57, 9.42, 8.46, 20.49, and 12.36 for 1995, 1996, 1997, 1998, and 1999 respectively, which is statistically significant with a credibility of 99%. Thus, we can conclude that the Israeli side is generally hotter. The anomalous LST difference is very obvious in the hot dry season, when the Israeli side is about 2.5–3.5°C hotter. In the cool wet season, the difference still exists but reduces to less than 1.5°C.

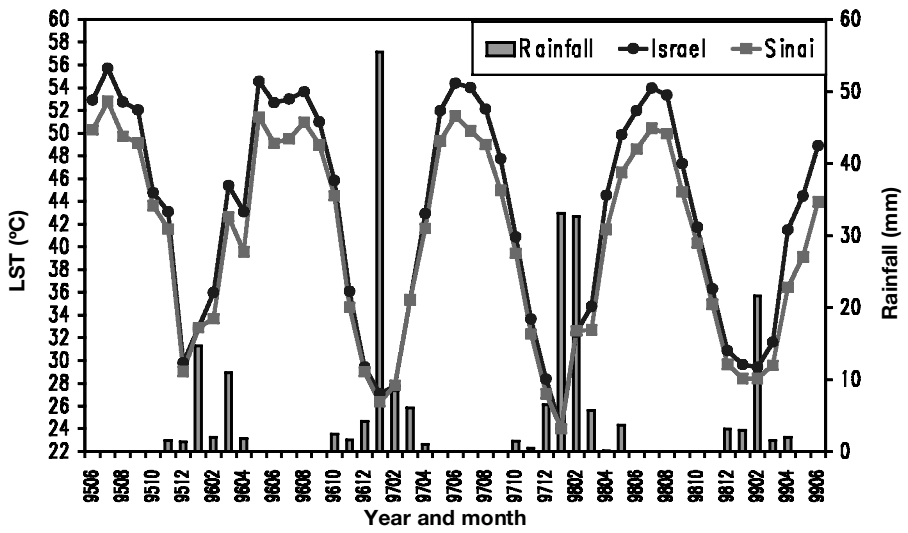

Figure 8. Comparison of average monthly LST change with rainfall on both sides of the region.

4.2. *Night-time LST change and its difference on both sides*

Night-time images in the region in 1998 were also selected for analysis. The same methodology for LST retrieval from daytime images was applied to process the night-time images. Figure 9 shows the night-time average LST change and its difference on the two sides of the region. The temporal change of night-time LST has similar features as the daytime. Night-time LST during the hot dry season is generally higher than the cool wet season. Figure 9(a) shows that the average LST change at about midnight is within the range of 20–26°C in the hot dry season and about 10–15°C in the cool wet season.

However, the obvious LST difference on both sides in the daytime images cannot be seen in the night-time images. As shown in figure 9(b), the magnitude of the night-time LST difference is generally within ± 0.75°C, which is quite small compared with the sharp contrast in daytime. Moreover, the difference is not regular. Sometimes

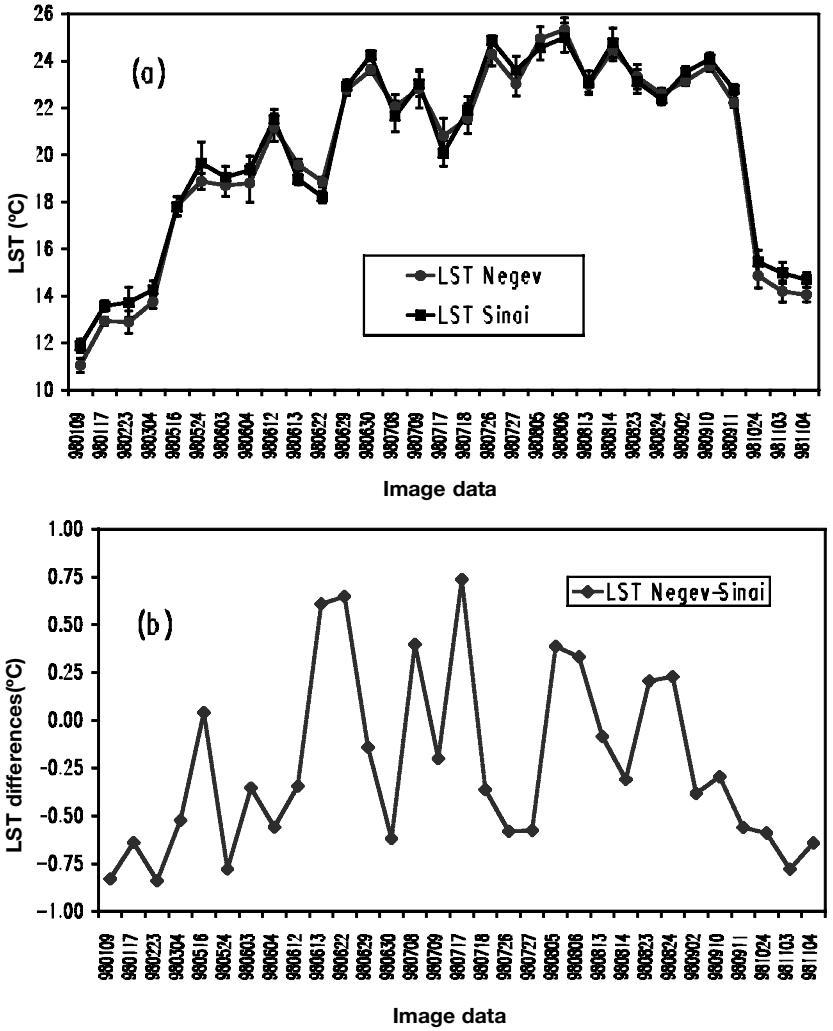

Figure 9. Night LST change on both sides of the region, retrieved from selected NOAA-AVHRR night images of 1998. (a) Average LST change, (b) average LST difference.

the Israeli side has higher LST while sometime the opposite can be seen. Therefore, the conclusion can be drawn that the obvious LST difference during daytime in summer disappears during night-time. The T-test indicates that $T_{stat} = 0.62$ for the LST difference between May and August, which is not significant at the level $\alpha = 0.1$. However, the T-test indicates that the Egyptian side is hotter in winter (statistically significant at $\alpha = 0.01$) though the average night-time LST difference is only about 0.5–0.8°C between the two sides.

5. Spatial distribution of LST in the border region

We applied the above mono-window algorithm to retrieve LST from available Landsat TM6 data of the region. Figure 6(b) shows the result of this retrieval, i.e. the spatial variation of LST distribution in the border region. This image was taken on 21 September 1995 during the late dry season. The satellite Landsat-5 passed the area at about 09:45 local time. A clear difference in LST between the two sides can be seen in this image. Generally the Israeli side has higher LST. On average, LST is 38°C on the Israeli side and 36°C on the Egyptian side. Thus, the difference is about 2°C in the mid-morning. High LST can be seen on the Israeli side in the right upper part of the image. The LST in this area is above 40°C. Low LST concentrates in the middle part of the Egyptian side. The LST in this part is around 35°C. Thus, the maximum LST difference is 5°C. This contrast of LST distribution on the two sides makes the border very clear in the sand-dune region (figure 6(b)). The landscape in the lower right portion of the image consists of mainly rocky terrain patterns. The lowest LST can be found in the wadi (flood river valley) crossing the terrain where shrubs dominate the surface.

Considering the higher vegetation cover on the Israeli side, its higher LST is an interesting anomaly. The reason is that the Israeli side has much higher biogenic crust cover rate while the Egyptian side has much more sand surface. Biogenic crust cover rate on the Israeli side is estimated to be approximately 72%, and sand surface on the Egyptian side is above 80% (see §7). The biogenic crust usually has much higher surface temperature than sand (see §6). Our ground truth measurements indicate that surface temperature on the biogenic crust is more than 3°C higher. Therefore, the higher LST on the Israeli side is due to the contribution of biogenic crust overcoming the cooling process of its vegetation cover. Detailed examination of this mechanism from the viewpoint of micrometeorological modelling has been addressed in another article (Qin *et al.* 2002).

We also have several other TM images of this region. Though these images do not have full cover of both sides, they still can be used to analyse the LST change of the region. After LST retrieval, we calculated the average LST on both sides for each image and the result is shown in figure 10, which depicts the average LST change and its difference across the border. Several features can be seen in this graph. In the hot dry season, LST of the region is up to around 50°C at approximately 10:00 local time. In the early and late dry seasons the LST is around 40°C. However, it is very low (about 20°C) in the cool wet season. The LST difference between the two sides is obvious in the dry and late wet seasons. Usually the Israeli side has an average LST of >2°C higher than the Egyptian side. The sharp LST difference disappears in the cool wet season when the temperature is below 25°C. The anomalous thermal variation on both sides is governed by the seasonal change of the local climatology, which couples with moisture variation in the soil and the air. When the

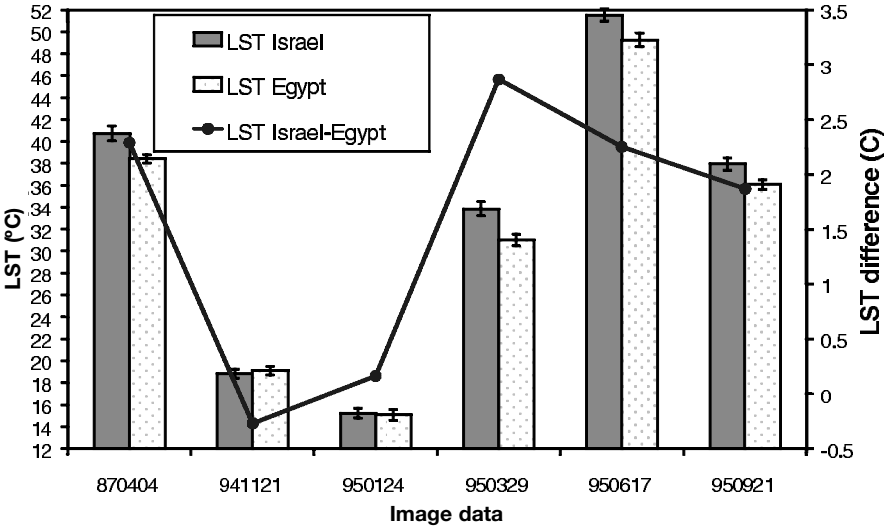

Figure 10. Average LST change on both sides and their difference, retrieving from Landsat TM images.

temperature is lower than a level such as 20°C, the Israeli side does not have higher, but instead slightly lower, LST.

6. Ground truth measurements of surface temperature change

The above remote sensing analysis indicates that the border region does have sharp contrast of LST change during the day, even though the phenomenon fluctuates in different seasons. In order to validate the observed LST contrast on remote sensing data, we performed ground truth measurements at Nizzana Research Site on the Israeli side (see figure 6(b)). Field investigation indicates that the surface of the region can be viewed as composed of four main patterns: biogenic crust, sand, playa and vegetation. Therefore, it is natural to think that the LST difference observed by remote sensing on the two sides directly results from the difference of surface composition structure. Moreover, the fact that the ground of the Israeli side is mainly covered with biogenic crust and various shrubs while that of the Egyptian side is dominantly sand (Danin *et al.* 1989, Pinker and Karnieli 1995, Karnieli 1997). Thus, it can be logically concluded that there would be an obvious kinetic surface temperature (KST) difference among the surface patterns.

Measurements were carried out using a hand-held IR thermometer operating in the spectrum of 8–14 μm. The output of the thermometer is radiant surface temperature (RST). The advantage of using a radiant thermometer for the measurements is that it has the ability of rapidly (usually in about two seconds) responding to thermal emission of the measured target and the output is parallel to that obtained in remote sensing. The output frequency of the thermometer can reach one record per second.

Several measurements were performed during 1997–1998. A number of sampling sites representing the main surface patterns had been selected for the measurements as ground surface temperature changes from time to time and we have only one thermometer. In order to obtain comparable results, the adjacent sampling sites in

a small area were selected. At each sampling site, the thermometer was pointed to the ground at the height of about 1 m with a viewing angle close to nadir. The actual measuring time for each site was about 20 seconds. The recorded data was loaded onto a computer and the average RST was computed for each sampling site. Based on Stefan-Boltzmann radiation law, KST can be computed from RST using the following formula:

$$T_k = \sqrt[4]{\frac{\sigma T_r^4 - (1-\varepsilon) I^{\propto}}{\varepsilon \sigma}} \tag{18}$$

where T_k and T_r are KST and RST respectively, with dimension in K, ε is emissivity, σ is Stefan-Boltzmann constant ($5.67 \times 10^{-8}\,\mathrm{W\,m^{-2}\,K^4}$), and $I\downarrow$ is downward sky radiance, which is determined by a number of atmospheric quantities such as air temperature, water vapour content and so on. For a clear sky with low water vapour content such as the arid region under study, $I\downarrow$ is usually less than $0.2\,\mathrm{Wm^{-2}}$. Consequently, the term $(1-\varepsilon)I\downarrow$ is very small (numerically <0.008) in comparison to the term σT_r^4 (numerically >8). Thus, the computation can be further simplified: $T_k = \varepsilon^{-1/4} T_r$ with a slight overestimate ($<0.1^{\circ}\mathrm{C}$) of T_k. For convenience, the emissivity used in the correction was as follows: 0.97 for biogenic crust, 0.95 for sand, 0.965 for playa and 0.975 for green vegetation. This estimation is reasonable according to our experiments and the literature (Takashima and Masuda 1987, Humes *et al.* 1994, Price 1984). The corrected results of the ground truth measurements are presented in figure 11 and table 2.

The results of ground truth measurements confirm what we expected according to the observed LST change on the two sides of the border region in remote sensing images. Though the analysis is based on the sampling sites, an obvious difference of surface temperature does exist between biogenic crust and sand in most days of the year. In the hot dry season at about noon, biogenic crust has higher KST than sand and the KST difference between them is above 3°C (figure 11(a)). The difference is also obvious in the morning and afternoon. Measurement on 18 June 1997 indicates that average KST is 43.6°C for crust and 41.5°C for sand. In the early and late dry seasons, the difference is still above 2.5°C (table 2). The situation reverses only in the several days of heavy rain when the crust is very wet or at a level of high water content while the sand is relatively drier. There was a heavy rain (23.9 mm) between 11 and 12 January 1998. The KST shown in figure 11(b) was measured after five days of the heavy rain. Under these extremely wet conditions, the sand surface has a KST of approximately 1°C higher than the crust. The lower KST of the crust is because soil-water content strongly shapes the thermal properties that govern KST change. Also the rain means that soil-water content increases. However, the reverse KST difference between the two main surfaces becomes very weak after about two weeks of strong rain, when the measurement was conducted on 25 January 1998 (table 2). Therefore, in the wet season, the biogenic crust has higher KST on most days except rainy days and a few days after the rain.

Plants have the lowest canopy temperature. In the hot dry season, the difference between shrub canopy temperature and biogenic crust KST may be up to 13°C at local noon, as indicated in table 2. During the wet season when the KST difference between biogenic crust and sand surface reverses due to the wetter of biogenic crust surface, shrub canopy temperature still remains about 3°C lower than the KST of sand, as on 16 January 1998.

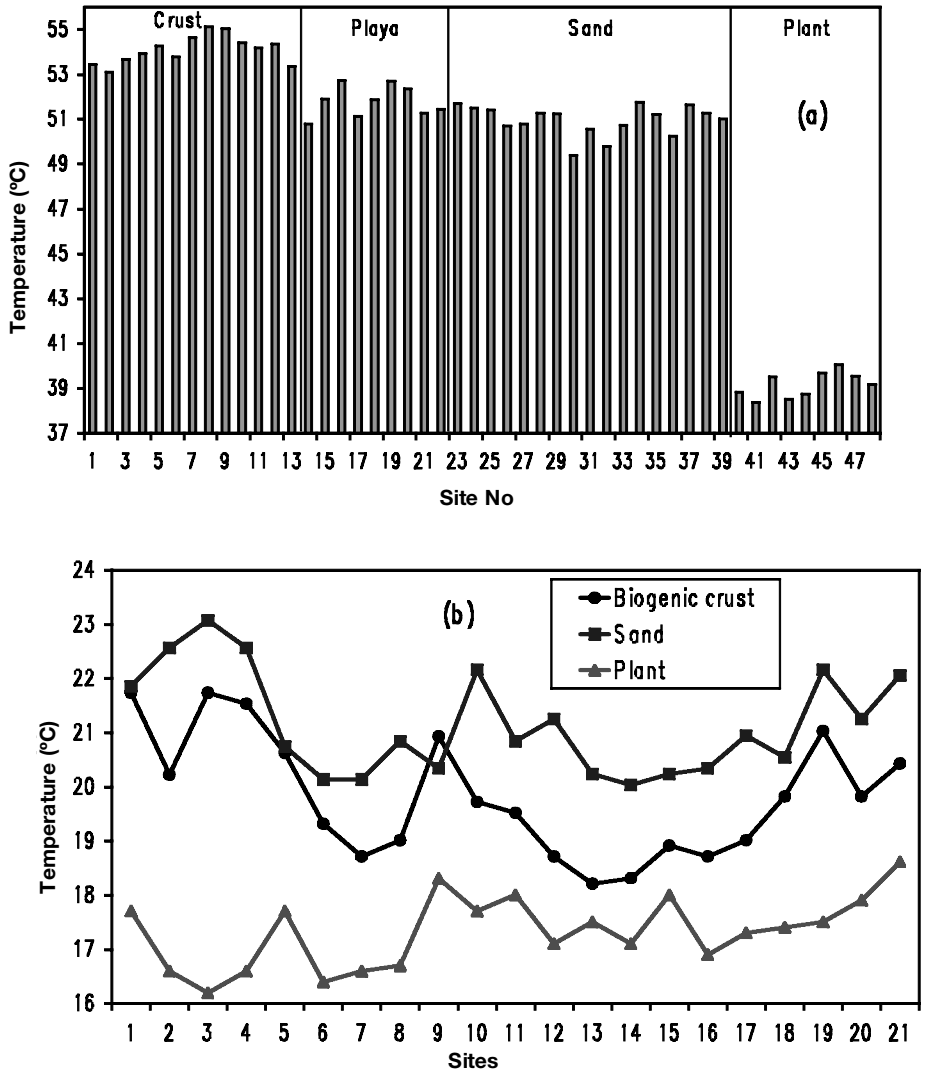

Figure 11. Surface temperature change of typical surface patterns, illustrating the measurements (a) in the dry hot season at 13:32–14:05 on 18 June 1997 and (b) in the very wet cool season at 09:00–09:25 on 16 January 1998 (local times). The number in the graph is the average KST of the patterns.

The ground truth measurements can also inform us of the possible extent which the KST of the main surface patterns may reach in various seasons. In the hot dry season, the KST of the biogenic crust may reach 52–55°C at about local noon. The KST of sand and playa may be up to 50–53°C and 51–53°C, respectively. Shrub canopy also has high temperature at noon in summer. In the wet cool season, the KST of biogenic crust and sand may reduce to below 20°C in a week after strong rain and the shrub canopy temperature may drop to about 16–17°C under these conditions. However, if there is no rain in about two weeks, the KST of biogenic crust and sand will recover to the level of >22–25°C. Usually the KST of biogenic crust is up to 38–40°C at local noon in the late wet season. The sand surface and

Table 2. Average KST of typical surface patterns in the region.

Measurement time	No.	Sampling sites	Average KST (°C)			
			Crust	Sand	Playa	Plant
13:32–14:05, 18 June 1997	M1	47	54.11	50.97	51.80	39.16
11:30–12:15, 1 August 1998	M2	49	51.97	49.39	50.09	38.88
16:15–16:48, 18 June 1997	M3	38	54.11	41.49		
4:15–14:52, 7 May 1997	M4	43	48.69	45.31	46.47	35.93
15:39–16:05, 7 May 1997	M5	37	43.27	40.58	41.96	33.82
14:19–14:55, 6 October 1997	M6	45	43.29	40.13	40.80	33.57
09:00–09:25, 16 January 1998	M7	63	19.39	20.89		17.51
10:00–10:35, 25 January 1998	M8	45	22.75	23.10		18.57
11:20–12:00, 19 March 1998	M9	47	35.64	33.41	34.36	25.64
11:16–12:04, 26 March 1998	M10	45	34.55	31.71	32.55	26.27
10:30–11:11, 10 April 1998	M11	56	36.32	34.50		27.44

shrub canopy in the season may have KST of 35–37°C and 27–30°C, respectively. Knowledge of these changes is important for simulating the mixed KST difference on both sides of the region, because we cannot cross the border to take any measurements on the Egyptian side.

7. Estimation of surface composition structure

Considering the lithological and geomorphological similarity on both sides, the sharp contrast of LST across the border can be interpreted as being caused by the difference of the surface composition structure. Thus, estimation of land cover on the two sides is necessary for understanding the generation of this abnormal thermal phenomenon.

As indicated above, the region can be viewed as composed of four main surface patterns: biogenic crust, sand, vegetation and playa. The accurate percentage of each pattern has not yet been reported, though several studies (Otterman 1974, 1977, 1981, Tsoar and Møller 1986, Karnieli 1997) found more vegetation cover on the Israeli side. Kidron and Yair (1997) arbitrarily guessed 10–40% of vegetation cover, Karnieli and Tsoar (1995) lower than 30% in the region and Otterman and Robinove (1982) about 20% on the Israeli side. Details of plant communities at the Nizzana Research Site was investigated by Tielbörger (1997), who also reported the percentage cover of each perennial plant communities at the site, ranging from 1.9% in Anabasis articulata to 32.1% in Noaea mucronata-Artemisia monosperma. The exact percentage of other surface patterns such as biogenic crust and sand has not yet been reported.

We used three methods to estimate the cover rate of surface patterns in the region: field observation, measuring on aerial photograph and Landsat TM image. Field observation was carried out on 26 March 1998 at the Nizzana Research Site (see figure 6(b)). The primary purpose is to determinate the vegetation cover rate. Five plots with various landscapes were selected for the observation. Two plots are in the interdune, one at the foot of dune slope, one in the middle and one on the top of dune. The surface of the sampled plots mainly constitutes biogenic crust and vegetation (mainly shrubs) except the plot on top dune, which has the structure of sand and vegetation. First, the size of each plot was measured and the total number of shrubs was counted. Then, a number of shrubs were randomly selected and their

diameter measured, because measuring all the shrubs is a time consuming process. Finally, the average diameter was calculated for estimating total vegetation area. The rate of vegetation cover is given by dividing vegetation area by the total.

The aerial photograph for the measurement covers both sides and has three channels in the visible range. The method used for measuring vegetation cover rate on the image includes making subsets for both sides and measuring the land cover patterns on them. The vegetation shrubs appear as low DN (digital number) value pixels and sand surface as high DN value pixels in all three channels. Playa also has high DN value. The DN value of biogenic crust is between that of vegetation and sand. Because both supervised and unsupervised classifications with all three channels cannot give good results, we decided to firstly classify the shrubs from other patterns on channel 1, then to use interpretation method to identify the other three patterns. On the Egyptian side, bare sand is the prevalent surface pattern and biogenic crust and playa are distributed as plots. Therefore, the areas of biogenic crust and playa plots were measured and the rest was designated bare sand. On the Israeli side, biogenic crust is dominant. The areas of bare sand and playa were firstly measured and the rest was designated biogenic crust. The shrub area on the measured plots was subtracted from the area of the measured plots. The cover rate for each surface pattern was calculated as the ratio of its area to the total.

The TM image used for the estimation was acquired on 29 March 1995, during the vegetation blooming period. Based on the spectral characteristics of vegetation, vegetation cover rate (R_v) can be calculated from the normalized difference of vegetation index ($NDVI$) as follows (Kerr *et al.* 1992):

$$R_v = (NDVI - NDVI_b)/(NDVI_v - NDVI_b) \tag{19}$$

where $NDVI_v$ is the maximal $NDVI$ of a fully vegetated surface and $NDVI_b$ is the minimal $NDVI$ of a pure background surface having no vegetation. Thus, the accuracy of using $NDVI$ to determine vegetation cover rate will depend on the two coefficients $NDVI_v$ and $NDVI_b$. Usually, the reflectance of green vegetation is very low in red and very high in infrared (Barett and Curtis 1978, Cracknell and Hayes 1993). According to the measurement of Tsoar and Karnieli (1996) to the spectra of desert shrub (Artemisia) in the region, $NDVI_v$ is estimated to be about 0.60. The surface of the region is mainly covered with sand and biogenic crust (mainly cyanobacteria crust). According to the reflectance of cyanobacteria crust and sand in Karnieli *et al.* (1996), $NDVI$ is estimated to be about 0.036 for sand and about 0.055 for cyanobacteria crust. Due to surface composition difference on both sides, we would like to use the $NDVI$ for cyanobacteria crust as the $NDVI_b$ on the Israeli side and for sand as the $NDVI_b$ on the Egyptian side.

Results from field observation indicate that, on average, vegetation covers about 15.63% of the sand-dune region on the Israeli side, biogenic crust 69.423%, sand 11.935% and playa 3.012%. These results are based on the statistical analysis of the total sampling area of 3851 m^2. The results from measurement of the aerial photograph indicate that a sharp contrast of vegetation cover exists between the Israeli side and the Egyptian side. Vegetation covers about 17.02% on the Israeli side and 5.81% on the Egyptian side. Biogenic crust occupies about 68.28% on the Israeli side and 18.03% on the Egyptian side. Bare sand covers about 11.19% on the Israeli side and 72.45% on the Egyptian side. Playa covers only a small percentage on both sides: 3.50% on the Israeli side and 3.72% on the Egyptian side.

Observation of the photograph reveals that the vegetation density and biogenic

crust area on the Egyptian side vanish rapidly with distance from the border. Results from sampling on three strips indicate that sand cover increases from 42.45% in strip 1 (near the border) to 71.35% in strip 3 while crust cover drops from 43.59% in strip 1 to 18.03% in strip 3. Vegetation cover also drops from 11.44% in strip 1 to 5.91% in strip 3. Since strip 3 is only about 0.8 km from the border, we can logically expect a higher average sand cover on the Egyptian side.

Results from measurement of the TM image indicate that the vegetation cover rate is 17.53% on the Israeli side and 5.15% on the Egyptian side. Based on the three methods of measurement, we estimate the surface composition structure of the region as follows. On average, the vegetation cover rate is about 17.5% on the Israeli side and 4.5% on the Egyptian side. Biogenic crust occupies about 72% of the surface on the Israeli side and 12% on the Egyptian side. Bare sand covers about 7% on the Israeli side and 80% on the Egyptian side. The playa accounts for 3.5% on both sides.

8. Surface composition structure and LST change on the two sides

Because the ground surface is a mixture of various patterns, the LST retrieved from remote sensing images cannot be directly correlated with what we have learned about KST change through ground truth measurements on different surface patterns. In order to understand the relationship between ground truth measurements and remote sensing observation, consideration of ground composition structure is necessary.

8.1. *Analysis framework*

The combination of the four surface patterns has a sharp difference between the two sides of the border region. It has been assumed that this difference is the direct reason for the sharp change in LST observed by remote sensing. Actually, the LST retrieved from remote sensing images is a mixed surface temperature, which can be divided into several components according to the surface composition structure. For the study region, total thermal radiance (I_s) emitted from the ground can be written as:

$$I_g = A_c I_c + A_s I_s + A_v I_v + A_p I_p \tag{20}$$

where A_c, A_s, A_v, and A_p are surface fractions of biogenic crust, sand, vegetation and playa, respectively, and I_c, I_s, I_v, and I_p are the thermal radiance emitted from the four surface patterns. Applying the Stefan-Boltzmann law of radiance to the above equation, we get:

$$\varepsilon\sigma T_s^4 = A_c\varepsilon_c\sigma T_{kc}^4 + A_s\varepsilon_s\sigma T_{ks}^4 + A_v\varepsilon_v\sigma T_{kv}^4 + A_p\varepsilon_p\sigma T_{kp}^4 \tag{21}$$

where σ is Stefan-Boltzmann constant, T_s is the average LST, T_{kc}, T_{ks}, T_{kv}, and T_{kp} are KST of biogenic crust, sand, vegetation and playa, respectively, and A_c, A_s, A_v, and A_p are the surface fraction of the four patterns. In fact, the sum of the surface fractions is equal to 1 (i.e. $A_c + A_s + A_v + A_p = 1$) ε is the average ground emissivity, which in our case can be approximated as:

$$\varepsilon = A_c\varepsilon_c + A_s\varepsilon_s + A_v\varepsilon_v + A_p\varepsilon_p \tag{22}$$

Elimination of σ from equation 27 leads to the following formula for calculation of average LST in the region:

$$T_s = (F_c T_{kc}^4 + F_s T_{ks}^4 + F_v T_{kv}^4 + F_p T_{kp}^4)^{1/4} \tag{23}$$

where the coefficients F_c, F_s, F_v, and F_p are the emissivity fractions, given by $F_c = A_c\varepsilon_c/\varepsilon$, $F_s = A_s\varepsilon_s/\varepsilon$, $F_v = A_v\varepsilon_v/\varepsilon$, and $F_p = A_v\varepsilon_v/\varepsilon$. During the hot dry season, most vegetation (shrub) in the region is in dormancy and the canopy of vegetation reduces to its minimum. Field observation reveals that the shrub canopy can cover as low as one third of its ground shadow. This implies that radiance from the shrub canopy shadow is mixed, combining vegetation emittance and ground emittance. Threrefore, the emissivity fraction can be estimated for each surface pattern. Consequently, it is possible to analyse the impact of surface composition on LST change and compare the difference between the two sides of the region.

8.2. *Impact of surface composition and ground emissivity on LST change*

Because the surface is composed of four patterns and each pattern has its own specific ground emissivity, average LST surface temperature on the two sides is in fact impacted by the combination of these two factors: surface composition and ground emissivity. Figure 12 shows the estimated combination impact of these two factors on the average LST difference between the two sides. Two features can be clearly seen. The Israeli side has a higher average LST when the biogenic crust has a KST of >1°C higher than sand. In summer, surface temperature of the region is usually in the range of 40–57°C at about local noon during the day. As indicated in ground truth measurements, biogenic crust is usually above 3°C hotter than bare sand. In these conditions, the average LST difference on both sides will be >2.5°C. In other words, the Israeli side is approximately 2.5°C hotter (figure 12). This is in accordance with the remote sensing analysis of LST change retrieved from AVHRR and Landsat TM data.

In winter and during night, surface temperature of the region is usually low. The difference of surface temperature between biogenic crust and bare sand is not as obvious as under hot dry conditions. As shown in figure 12, the average LST difference on both sides is -0.6°C when the biogenic crust is about -1°C cooler than bare sand. This implies that at low temperatures, such as for several days after

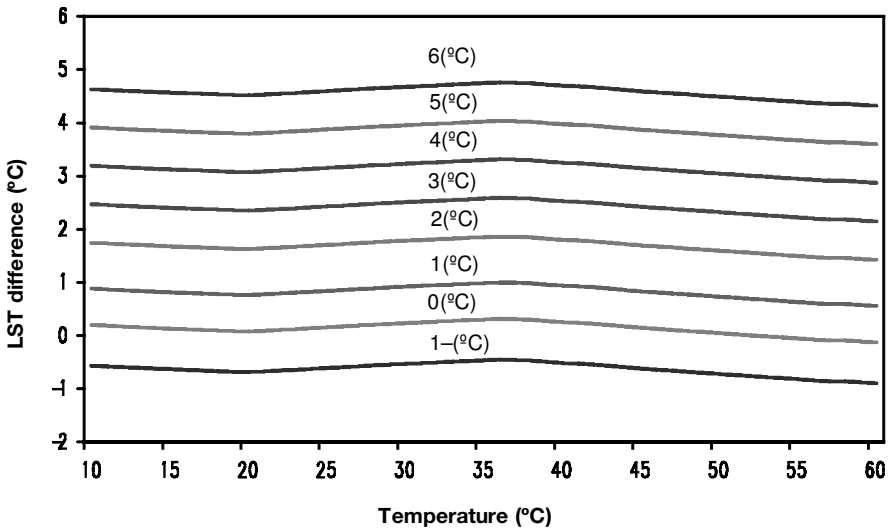

Figure 12. Impact of KST difference between biogenic crust and bare sand on average LST difference on both sides of the region.

rain and during winter night-time the Egyptian side probably has slightly higher LST. However, if biogenic crust and sand have no difference in their surface temperatures, the Israeli and the Egyptian sides will also have no significant LST difference in average. This result also validates the remote sensing analysis of the LST change on the two sides.

8.3. *Possible average LST change and its difference on both sides*

On the basis of the above analysis, the average LST change and its difference on both sides of the region were simulated with equation 23 under possible temperature changes of the main surface patterns. The results shown in figure 13(a) indicate that the average LST on the two sides of the region changes from about 10°C to 59°C

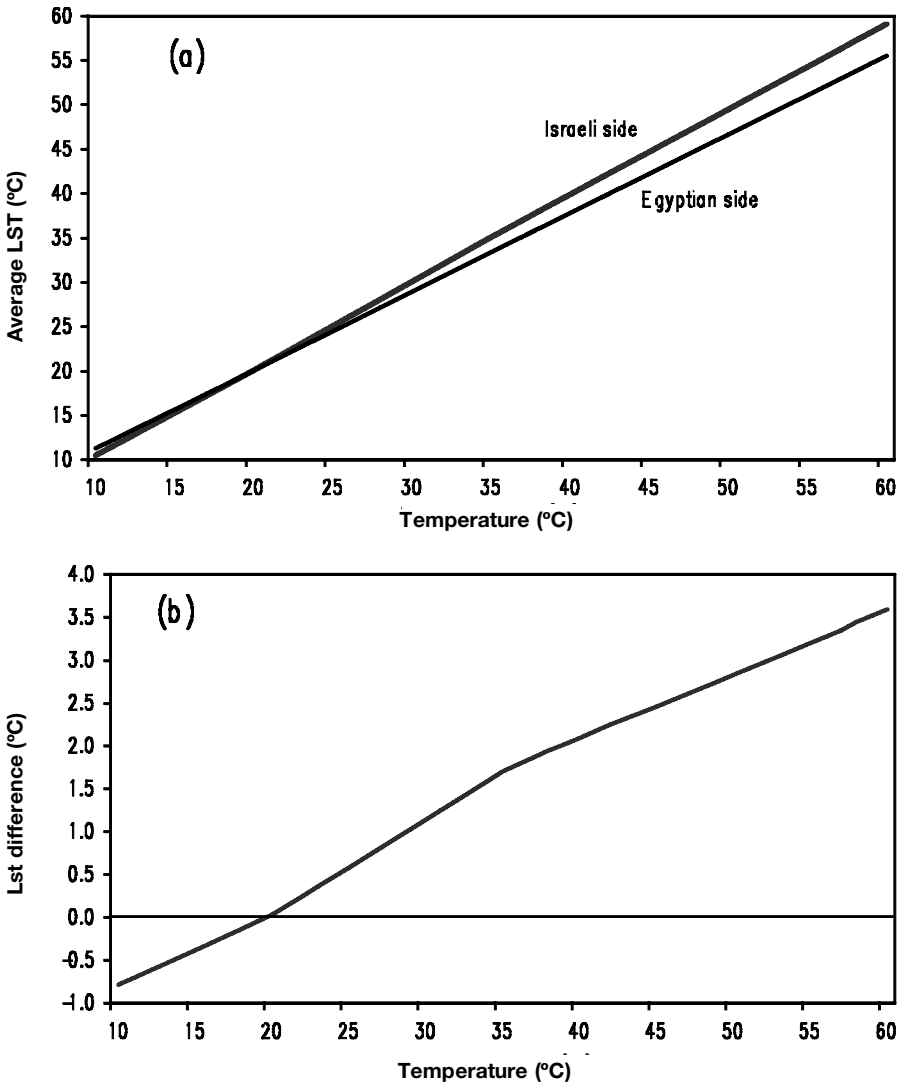

Figure 13. Possible average LST change (a) and its difference (b) on the two sides of the region, simulated by surface composition and ground emissivity.

in correspondence with the temperature range (10–60°C) of biogenic crust. The linear characteristic of the change is obvious. Generally, the Israeli side will have higher average LST at high temperature levels such as >30°C. At low temperature levels, e.g. <15°C, the Egyptian side may have steadily higher average LST though the difference is still weak (< −1°C). Another important feature shown in figure 13(a) is that average LST difference on both sides is not obvious, vibrating between −0.5°C and 0.5°C, in the temperature range 15–25°C. Usually LST of the region is within this range at about midnight. This is why we cannot observe an obvious LST anomaly of the region on the night-time remote sensing images of AVHRR, as indicated in §5. The change of possible average LST difference between the two sides is clearly shown in figure 13(b). Specifically, LST difference between the Israeli side and the Egyptian may reach 2.5–3.5°C when the temperature level is in the range of 45–55°C, which is the general case during hot dry season.

8.4. *Average LST change and its difference on both sides near the border*

Based on the ground truth measurements shown in table 2, the average LST change on both sides and their difference is estimated, which leads to the results shown in figure 14. According to the measurement M1, the average LST is 53.6°C on the Israeli side and 51.2°C on the Egyptian side, with a difference of 2.4°C. The average LST on both sides is 2.1°C according to M2, the measurement taken before noon. Because the measurement shown in M3 was taken in late afternoon, the lower average LST difference on both sides (1.9°C) is reasonable. Similar LST difference on both sides can be seen in early and late dry seasons. For the cases of M4–6, average LST difference is found to be high—up to 2.3–2.7°C (figure 14). However, the reverse LST difference on both sides exists in the cool wet season when temperature is lower. As indicated in figure 13(b), the average LST on the two sides may have an insignificant difference when the temperature is around 20°C, which is

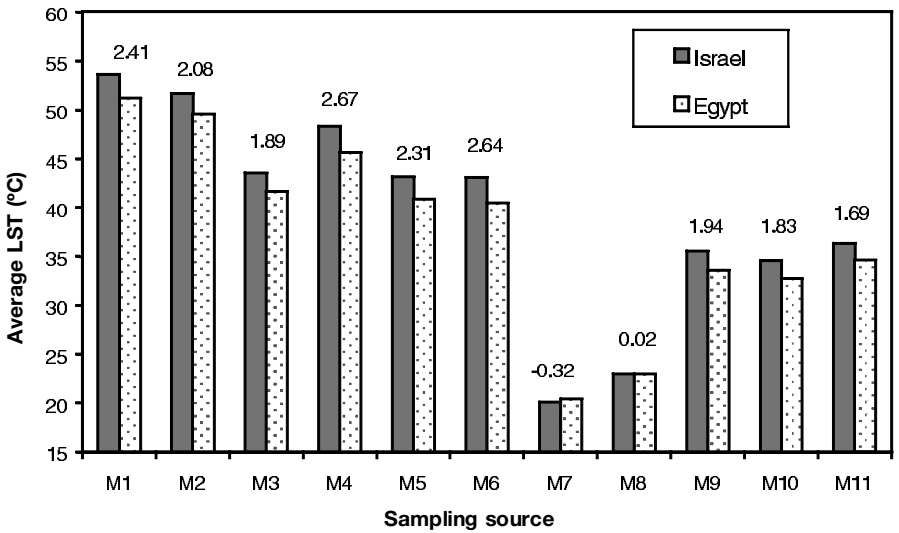

Figure 14. Average LST change on the two sides of the region, estimated from the ground truth measurements taken at the Nizzana Research Site. The number in the graph is the LST difference on both sides. Sampling source refers to table 2.

validated in the ground truth measurements M7–8. Due to very wet surfaces after heavy rain, the average LST on M7–8 is estimated to be about 20°C and 23°C on both sides. Consequently, the LST difference on both sides is −0.3°C and 0°C, respectively.

9. Conclusion

The characteristics of average LST and its variations have been simulated and analysed according to the surface composition structure on both sides of the region. First we estimated the average LST difference on the two sides for various LST differences between biogenic crust and bare sand. Then, the average LST change on the two sides was computed according to the possible LST change of the four typical surface patterns. Finally, the estimation method of average LST change on both sides was applied to the ground truth measurements taken on the Israeli side.

On average, it can be firmly concluded that the Israeli side will have a higher LST than the Egyptian side if the biogenic crust is more than 1°C hotter than sand, which occurs at moderate to high temperature levels. Generally, we can expect an average LST difference of 2.5–3.5°C between the Israeli and the Egyptian sides at around local noon during summer season when temperature is 45–55°C. For low temperature in winter after rain, the Egyptian side probably has a slightly higher average LST. When the temperature is around 20°C, the two sides will have insignificant average LST difference. These simulation results explain why the sharp LST contrast on both sides can be observed in the daytime images acquired at around 14:00 (AVHRR) and 09:30 (Landsat TM) but can not be seen in night-time images acquired at around midnight.

Since the simulation is based on different surface composition, it can therefore be concluded that the obvious LST difference across the border is mainly due to the difference of surface composition structure on both sides. This surface composition difference together with the emissivity difference among the components plays an important role in shaping LST change on both sides of the region. The Israeli side has about 72% surface covered with biogenic crust while the Egyptian side has more than 4/5 surface covered by bare sand. Ground truth measurements validated that biogenic crust has a higher surface temperature than bare sand. The much greater fraction of biogenic crust on the Israeli side determines its much higher average LST change. The greater fraction of bare sand on the Egyptian side explains its lower average LST change. Even though there is a sharp difference of vegetation cover rate on both sides, this has a proportionately low contribution to the differences in the average LST across the border.

Acknowledgments

The authors sincerely thank the following for their help in the research presented here: Dr Heike Schmid, our colleague at the Remote Sensing Laboratory, for helping to access the region for ground truth measurements; Mr Giorgio Dall'Olmo, our colleague, for assistance in image processing; Mr Simon Berkowics, administrator of the Arid Econsystems Research Center, Institute of Earth Sciences, the Hebrew University of Jerusalem, for offering the permission to conduct ground truth measurements at the Nizzana Research Site and providing rainfall data of the region; and Prof. Natan Kopeika, Ben Gurion University of the Negev, for allowing us to use his LOWTRAN 7 program for atmospheric simulation.

References

Bahre, C. J., and Bradbury, D. E., 1978, Vegetation change along the Arizona–Sonora boundary. *Annals of the Association of American Geographers*, **68**, 145–165.

Balling Jr., R. C., 1989, The impact of summer rainfall on the temperature gradient along the United States–Mexico border. *Journal of Applied Climatology*, **28**, 304–308.

Balling Jr., R. C., Klopatek, J. M., Hildebrandt, M. L., Moritz, C. K., and Watts, C. J., 1998, Impacts of land degradation on historical temperature records from the Sonoran desert. *Climatic Change*; **40**, 669–681.

Barrett, E. C., and Curtis, L. F., 1978, *Introduction to Environmental Remote Sensing* (New York: John Wiley & Sons Ltd).

Caselles, V., Coll, C., and Valor, E., 1997, Land surface emissivity and temperature determination in the whole HAPES-Sahel area from AVHRR data. *International Journal of Remote Sensing*, **18**, 1009–1027.

Coll, C., Caselles, V., and Schmugge, T. J., 1994a, Estimation of land surface emissivity differences in the split-window channels of AVHRR. *Remote Sensing of Environment*, **48**, 127–134.

Coll, C., Caselles, V., Sobrino, A., and Valor, E., 1994b, On the atmospheric dependence of the split-window equation for land surface temperature. *International Journal of Remote Sensing*, **15**, 105–122.

Cooper, D. I., and Asrar, G., 1989, Evaluating atmospheric correction models for retrieving surface temperatures from the AVHRR over a tall-grass prairies. *Remote Sensing of Environment*, **27**, 93–102.

Cracknell, A. P., and Hayes, L. W., 1993, *Introduction to Remote Sensing*. (London: Taylor & Francis).

Danin, A., Bar-Or, Y., Dor, I., and Yisraeli, T., 1989, The role of cyano-bacteria in stabilization of sand dunes in southern Israel, *Ecological Mediterranean*, **15**, 55–64.

Deschamps, P. Y., and Phulpin, T., 1980, Atmospheric correction of infrared measurements of sea surface temperature using channels at 3.7, 11 and 12 μm. *Boundary–Layer Meteorology*, **18**, 131–143.

França, G. B., and Cracknell, A. P., 1994, Retrieval of land and sea surface temperature using NOAA-11 AVHRR data in northeastern Brazil. *International Journal of Remote Sensing*, **15**, 1695–1712.

Humes, K. S., Kustas, W. P., Moran, M. S., Nichols, W. D., and Weltz, M. A., 1994, Variability of emissivity and surface temperature over a sparsely vegetated surface, *Water Resources Research*, **30**, 1299–1310.

Hurtado, E., Vidal, A., and Caselles, V., 1996, Comparison of two atmospheric correction methods for Landsat TM thermal band. *International Journal of Remote Sensing*, **17**, 237–247.

Karnieli, A., 1997, Development and implementation of spectral crust index over dune sands. *International Journal of Remote Sensing*, **18**, 1207–1220.

Karnieli, A., and Sarafis, V., 1996, Reflectance spectrophotometry of cyanobacteria within soil crusts—a diagnostic tool. *International Journal of Remote Sensing*, **17,** 1609–1615.

Karnieli, A., and Tsoar, H., 1995, Spectral reflectance of biogenic crust developed on desert dune sand along the Israel–Egypt border. *International Journal of Remote Sensing*, **16**, 369–374.

Karnieli, A., Shachack, M., Tsoar, H., Zaady, E., Kaufman, Y., and Porter, W., 1996, The effect of microphytes on the spectral reflectance of vegetation in semi-arid regions. *Remote Sensing of Environment*, **57**, 88–96.

Kerr, Y. H, Lagouarde, J. P., and Imbernon, J., 1992, Accurate land surface temperature retrieval from AVHRR data with use of an improved split window algorithm. *Remote Sensing of Environment*, **41**, 197–209.

Kidron, G. J., and Yair, A., 1997, Rainfall-runoff relationship over encrusted dune surfaces, Nizzana, Western Negev, Israel. *Earth Surface Processes and Landforms*, **22**, 1169–1184.

Labed, J., and Stoll, M. P., 1991, Spatial variability of land surface emissivity in the thermal infrared band: spectral signature and effective surface temperature, *Remote Sensing of Environment*, **38**, 1–17.

McMillin, L. M., 1975, Estimation of sea surface temperatures from two infrared window

measurements with different absorption. *Journal of Geophysical Research*, **36**, 5113–5117.

Otterman, J., 1974, Baring high-albedo soils by overgrazing: a hypothesized desertification mechanism. *Science*, **186**, 531–533.

Otterman, J., 1977, Anthropogenic impact on the surface at the Earth. *Climatic Change*, **1**, 137–155.

Otterman, J., 1981, Satellite and field studies of man's impact on the surface in arid regions, *Tellus*, **33**, 68–77.

Otterman, J., and Robinove, C. J., 1982, Landsat monitoring of desert vegetation growth in 1972–1979 using a plant shadowing model. *Advances of Space Research*, **2**, 45–50.

Otterman, J., and Tucker, C. J., 1985, Satellite measurements of surface albedo in semi desert. *Journal of Climate and Applied Meteorology*, **24**, 228–235.

Pinker, R. T., and Karnieli, A., 1995, Characteristic spectral reflectance of a semi-arid environment. *International Journal of Remote Sensing*, **16**,1341–1363.

Prabhakara, C., Dalu, G., and Kunde, V. G., 1974, Estimation of sea temperature from remote sensing in the 11 to 13 μm window region, *Journal of Geophysical Research*, **79**, 5039–5044.

Prata, A. J., 1993, Land surface temperature from the advanced very high resolution radiometer and the along-track scanning radiometer. 1. Theory. *Journal of Geophysical Research*, **98**, 16689–16702.

Prata, A. J., 1994, Land surface temperature from the advanced very high resolution radiometer and the along-track scanning radiometer. 2. Experimental results and validation of AVHRR algorithms, *Journal of Geophysical Research*, **99**, 13025–13058.

Price, J. C., 1984, Land surface temperature measurements from the split window channels of the NOAA 7 Advanced Very High Resolution Radiometer. *Journal of Geophysical Research*, **89**, 7231–7237.

Qin, Z., and Karnieli, A., 1999, Progress in the remote sensing of land surface temperature and ground emissivity using NOAA-AVHRR. *International Journal of Remote Sensing*, **20**, 2367–2393.

Qin, Z., Dall'Olmo, G., Karnieli, A., and Berliner, P., 2001a, Derivation of split window algorithm and its sensitivity analysis for retrieving land surface temperature from NOAA-AVHRR data. *Journal of Geophysical Research*, **106**, 22 655–22 670.

Qin, Z., Berliner, P., and Karnieli, A., 2001b, A mono-window algorithm for retrieving land surface temperature from Landsat TM data and its application to Israel–Egypt border region. *International Journal of Remote Sensing*, **22**, 3719–3746.

Qin, Z., Berliner, P., and Karnieli, A., 2002, Micrometeorological modeling to understand the thermal anomaly in the sand dunes across the Israel–Egypt border. *Journal of American Environment*.

Sobrino, J. A., and Caselles, V., 1991, A methodology for obtaining the crop temperature from NOAA-9 AVHRR data, *International Journal of Remote Sensing*, **12**, 2461–2475.

Sobrino, J. A., Coll, C., and Caselles, V., 1991, Atmospheric correction for land surface temperature using NOAA-11 AVHRR channels 4 and 5. *Remote Sensing of Environment*, **38**, 19–34.

Takashima, T., and Masuda, K., 1987, Emissivities of quartz and Sahara dust powers in the infrared region (1–17μm). *Remote Sensing of Environment*, **23**, 51–63.

Tielböger, K., 1997, The vegetation of linear desert dunes in the northwestern Negev, Israel. *Flora*, **192**, 261–278.

Tsoar, H., and Karnieli, A., 1996, What determines the spectral reflectance of the Negev-Sinai sand dunes. *International Journal of Remote Sensing*, **17**, 3513–3525.

Tsoar, H., and Møller, J. T., 1986, The role of vegetation in the formation of linear sand dunes. In *Aeolian Geomorphology*, edited by W. P. Nickling (Boston, MA: Allen & Unwin Inc.) pp. 75–95.

Vogt, J. V., 1996, Land surface temperature retrieval from NOAA-AVHRR data. In *Advances in the Use of NOAA-AVHRR Data for Land Applications*, edited by G. D'Souza, A. S. Belward and J.-P. Malingreau (Dordrecht, The Netherlands: Kluwer Academic Publishers), pp. 125–151.

Wan, Z., and Dozier, J., 1996, A generalized split-windows algorithm for retrieving land surface temperature from space. *IEEE Transactions on Geoscience and Remote Sensing*, **34**, 892–905.